Hindawi
Shock and Vibration
Volume 2018, Article ID 5131434, 13 pages
https://doi.org/10.1155/2018/5131434

Research Article

Online Classification of Road Roughness Conditions with Vehicle Unsprung Mass Acceleration by Sliding Time Window

Zhongxing Li,[1] **Wenhao Yu**,[1] **and Xiaoli Cui**[2]

[1]*School of Automotive and Traffic Engineering, Jiangsu University, Zhenjiang, China*
[2]*School of Automotive and Mechanical Engineering, Hunan Institute of Technology, Hengyang, China*

Correspondence should be addressed to Zhongxing Li; zhxli@ujs.edu.cn

Received 7 April 2018; Accepted 15 August 2018; Published 3 October 2018

Academic Editor: Francesco Pellicano

Suspension control systems are in need for more information of road roughness conditions to improve their performance under different roads. Existing methods of gauging road roughness are limited, and they usually involve visual inspections or special vehicles equipped with instruments that can gauge physical measurements of road irregularities. This paper proposes data collection for a period of a time from accelerometers fixed on unsprung mass and uses the mean square values of this datasets divided by vehicle speed to classify the roughness conditions of a section of a road. This approach is possible due to the existence of relationships between the power spectral densities of the road surface, unsprung mass accelerations via a transfer function, and vehicle speed. This paper gave the relationship between the resolution of road roughness classification and the length of time-window and suggestions about choosing the appropriate time-window length on the balance of road roughness resolution and classification delay. Moreover, to enhance the stability of classification, the influence of damping parameters of vehicle suspension on the classification output is studied, and a classification method of road roughness is proposed based on neural network and damping coefficient correction.

1. Introduction

Detection of road surface condition is important for numerous reasons, such as to improve the performance of some control systems [1, 2] and to apply different judgments on vehicle's actuators in different road conditions [3–5]. With the development of the vehicle control systems, it is becoming common practice that accelerometers are being installed on the suspension to upgrade suspension performance and to increase ride comfort. These accelerometers can measure the acceleration responses of vehicle unsprung and sprung masses to the road incentives. In this context, the acceleration data can be used to classify the average road conditions when vehicle suspension system is determined.

Existing methods for estimating road roughness can be divided into three categories [6]: direct measurements [7–11], noncontact measurements [12–15], and system response-based estimation [16–21].

Researchers who tried to measure and evaluate road roughness with direct measurements usually need either a special vehicle or sensors, which makes the method poor in portability. Recently, Japanese researchers Nuer-aihemaitijiang Abulizi et al. had proposed a road roughness estimator based on compact road profiler and ArcGIS [7], which services for the road management instead of systems on the vehicle; Russians researchers Lushnikov and Lushnikov used a profilometer that can measure the longitudinal microprofile of the road surface to assess the road surface roughness coefficients accurately [8]; Balaram and Mostert presented the results of road roughness measurements on a gravel road in KwaZulu-Natal collected with a Roughometer III [9], while Kumar et al. chose to use mobile laser scanning data to estimate the road roughness [10]. All the methods above need special sensors attached on the vehicles, but Zhang et al. developed a real-time roughness evaluation approach based on the durable in-pavement strain sensors that build in pavement panels [11]. Among these direct and noncontact measurements, they require either specific vehicles or sensors, which cause poor transplant ability and restrict their practical applications.

In the noncontact measurement method, Laubis et al. proposed a road condition estimation based on extended floating car data, which solves the problem of utilizing measurements from heterogeneous sources and can reduce the sensing frequencies while keep the performance [12]; Douangphachanh and Oneyama used smartphone sensors to estimate road roughness condition by frequency domain analysis, and an experiment had been conducted to support this method [13]; Tudon-Martinez et al. proposed a method of road profile estimation based on not only frequency but also amplitude estimation through an H_∞ robust observer, which shows only 16.97% error in the test [14]. Li et al. developed a method to detect the road based on airborne LiDAR point clouds, but LiDAR is very costly [15]. All the methods proposed need either large calculation to do frequency domain analysis or costly, which makes it difficult to make a low-cost scheme.

The last method is often used to estimate road excitation, and the estimation results can be further applied to adaptively changing control parameters, but usually they need a model with sufficient accuracy. Like Ngwangwa et al. used an artificial neural network simulation and vehicle dynamic response to classify road roughness and tested this method on the real measured data [16, 17]; Du et al. demonstrated a method using Z-axis acceleration with a one-wheel linear model and two-wheel model fitted to measure the road roughness [18]; Tudon-Martinez et al. proposed a method based on the Q-parameterization approach with vertical position of the sprung mass as the input and an adaptive observer estimating the road signal, a Fourier analysis to compute online road roughness [19, 20]; Gaspar et al. presented an identification method for the parameters of a quasilinear parameter varying medal and based on which, an autoregressive-moving average model structure was used to estimate road roughness [21].

Researches related to the road roughness estimation have been carried out in either time or frequency domains. But among those methods, the calculation is large, which requires too much computing time, and the relationship between accuracy and time consuming is not clear, or sensitive to the variety of suspension parameters. Estimating the road roughness is not the ultimate goal of this topic, but the meeting of other control systems' requirements on the vehicles. Thus, using specific sensors or equipment to measure the road roughness is undesirable; meanwhile, the estimation method should be oriented to different types of vehicles rather than a particular type of vehicle with small amount of calculation and convenient to arrangement.

In this paper, a novel method to classify road roughness based on unsprung mass acceleration is proposed, which overcomes the problems mentioned above and cater for those demands of the suspension control systems. This paper selected a classification parameter and proved the high correlation between this parameter and road roughness theoretically and then showed the contradiction of time consuming and the resolution of road roughness classification with this parameter for the convenience to choose the weight of them in practical application; next, the influence of sprung mass and damping coefficient were discussed, and a correct method was proposed for enhancing the transplant ability; finally, the results of using this parameter to classify was studied when applied to a vehicle with Sky-Hook controlled semiactive suspension on the condition of different road roughness coefficients.

2. Analysis of the Relationship between Unsprung Mass Acceleration and Road Roughness Coefficient

According to the International standard "ISO/TC 108/SC2N67," all kinds of road roughness with different grades are formulated and classified. The classification identifies eight-road roughness levels ranging from class A to H in increasing roughness order, where the first five classes (A~E) are important in practice. In the ISO (International Standards Organization) classification, the statistical characteristic of the road can be described by PSD, and the spatial frequency PSD $G_q(n)$ in m^3 can be approximated by

$$G_q(n) = G_q(n_0)\left(\frac{n}{n_0}\right)^{-W}, \quad n > 0, \tag{1}$$

where n is the spatial frequency in m^{-1}, which indicates the number of waves in every meter; n_0 is spatial reference frequency in m^{-1}, and usually, it equals to 0.1 m^{-1}; $G_q(n_0)$ is road roughness coefficient in m^3, which ranges from 16×10^{-6} to 262144×10^{-6} [22]; and its relationship with road roughness levels shown in Table 1. W is the frequency exponent. And usually, W equals 2 in road spectrum classification.

According to the vehicle speed, the spatial frequency PSD $G_q(n)$ can be converted into the circle frequency PSD $G_q(\omega)$. When the vehicle passes through a road with a spatial frequency of n (m^{-1}) at a certain speed v (m/s), the input circle frequency ω (rad/s) is as

$$\omega = 2\pi n v. \tag{2}$$

Assuming that the cut-off circle frequency is ω_0, we have,

$$G_q(\omega) = (2\pi)^2 G_q(n_0) n_0^2 \frac{v}{\omega^2 + \omega_0^2}. \tag{3}$$

The displacement PSD is usually calculated from the measurement of surface roughness described by vertical ordinates at an equally spaced point along the road. However, in the absence of such measurements, the circle frequency PSD of $G_q(\omega)$ can be generated as the response of a first-order linear system excited by white noise:

$$H(j\omega) = \frac{a}{b + j\omega}, \tag{4}$$

$$G_q(\omega) = |H(j\omega)|^2 S_\omega, \tag{5}$$

where $H(j\omega)$ is the first-order linear system and a and b are unknown parameters of this system. S_ω is the frequency PSD of white noise. According to Equations (3)–(5), the first-order linear system can be solved as

$$H(j\omega) = \frac{2\pi n_0 \sqrt{G_q(n_0) v}}{\omega_0 + j\omega}. \tag{6}$$

Table 1: Classification standards of road roughness.

Road roughness level	$G_q(n_0)$ value (m^3), geometric average
A	16×10^{-6}
B	64×10^{-6}
C	256×10^{-6}
D	1024×10^{-6}
E	4096×10^{-6}
F	16384×10^{-6}
G	65536×10^{-6}
H	262144×10^{-6}

Therefore,

$$G_q(\omega) = \left|\frac{2\pi n_0\sqrt{G_q(n_0)v}}{\omega_0 + j\omega}\right|^2$$
$$S_\omega = \frac{(2\pi n_0)^2 G_q(n_0) v(\omega^2+\omega_0^2)}{(\omega^2-\omega_0^2)^2} S_\omega. \quad (7)$$

For $\omega = 2\pi f$, the frequency PSD $G_q(f)$ can be described by

$$G_q(f) = \frac{n_0^2 G_q(n_0) v\left(f^2+f_0^2\right)}{(2\pi)^2\left(f^2-f_0^2\right)^2} S_\omega, \quad (8)$$

where f_0 is cut-off frequency. It approximated to a linear system when we discuss the vehicle vibration.

Because of the filtering effect of suspension system and frequent changes of sprung mass, the unsprung mass accelerations are chosen to be the data sources of this classification method, and in the quarter vehicle model, the PSD response of the unsprung mass acceleration $G_{a1}(f)$ has the following simplified relationship with the road displacement PSD $G_q(f)$ as

$$G_{a1}(f) = |H(f)|^2_{a1\sim q} G_q(f), \quad (9)$$

where $H(f)_{a1\sim q}$ is the frequency response of unsprung mass acceleration system $a1$ to input road displacement q, and $|H(f)|^2_{a1\sim q}$ is the model of this frequency response, namely, the amplitude-frequency characteristics.

Since the probabilities of the positive and negative responses of the vibration are the same, the mean value is approximately zero. Thus, variance, the statistical characteristic value of these quantities, equals mean square value σ^2 and can be obtained by integrating the PSD for the frequency as

$$\sigma^2 = \int_0^\infty G_{a1}(f)\, df = \int_0^\infty |H(f)|^2_{a1\sim q} G_q(f)\, df. \quad (10)$$

Based on the road displacement PSD $G_q(f)$ given by Equation (8), the mean square value of unsprung mass acceleration can be described by

$$\sigma^2 = \int_0^\infty |H(f)|^2_{a1\sim q} \frac{n_0^2 G_q(n_0) v\left(f^2+f_0^2\right)}{(2\pi)^2\left(f^2-f_0^2\right)^2} S_\omega$$
$$df = \frac{G_q(n_0) n_0^2 v}{(2\pi)^2} \int_0^\infty \frac{|H(f)|^2_{a1\sim q}\left(f^2+f_0^2\right)}{\left(f^2-f_0^2\right)^2} S_\omega\, df. \quad (11)$$

Obviously, the mean square of unsprung mass acceleration is strongly influenced by the road roughness coefficient $G_q(n_0)$ and the vehicle speed v when the parameters of vehicle system are determined.

2.1. Full Vehicle Model and Road Roughness Classification Parameters. To demonstrate the relationship between unsprung mass acceleration and road roughness coefficient under different vehicle speeds, a simplified linear pitch-plane 7 DOF (seven-degree of freedom) model was built for modeling the entire system, which comprises the vertical, roll, and pitch movement of the body and vertical movement of four wheels as shown in Figure 1.

Where, Z_{cg} is the vertical displacement of the body centroid; l_f and l_r are the distances from front and rear axles to the body centroid; M_b is the mass of the body; I_r is the rotational inertia of the body around the X-axis; I_p is the rotational inertia of the body around Y-axis; φ is the body roll angle, which is assumed positive when the body rolls toward the right side; θ is the body pitch angle, which is assumed to be positive when the body bends forward; K is the stiffness of each spring; c is the damping of each suspension; $Z_{ti}(i = 1, 2, 3, 4)$ are the vertical displacements of four wheels; M_t is the mass of each tire; K_t is the vertical stiffness of each tire; $q_i(i = 1, 2, 3, 4)$ are the vertical displacement excitations of four wheels respectively; and B_f, B_r are the distances between front and rear wheel tread, respectively.

The equation of motion of this linear vehicle model can be written as follows:

$$\begin{cases} M_b\ddot{Z}_{cg} = F_1 + F_2 + F_3 + F_4 - M_b\cdot g, \\ I_r\ddot{\phi} = \dfrac{B_f(F_2-F_1)}{2} - \dfrac{B_r(F_4-F_3)}{2}, \\ I_p\ddot{\theta} = (F_3+F_4)l_f - (F_1+F_2)l_r, \\ M_t\ddot{Z}_{t1} = K_t(q_1 - Z_{t1}) - F_1 + \dfrac{M_b\cdot g\cdot l_f}{(2(l_f+l_r))}, \\ M_t\ddot{Z}_{t2} = K_t(q_2 - Z_{t2}) - F_2 + \dfrac{M_b\cdot g\cdot l_f}{(2(l_f+l_r))}, \\ M_t\ddot{Z}_{t3} = K_t(q_3 - Z_{t3}) - F_3 + \dfrac{M_b\cdot g\cdot l_r}{(2(l_f+l_r))}, \\ M_t\ddot{Z}_{t4} = K_t(q_4 - Z_{t4}) - F_4 + \dfrac{M_b\cdot g\cdot l_r}{(2(l_f+l_r))}. \end{cases} \quad (12)$$

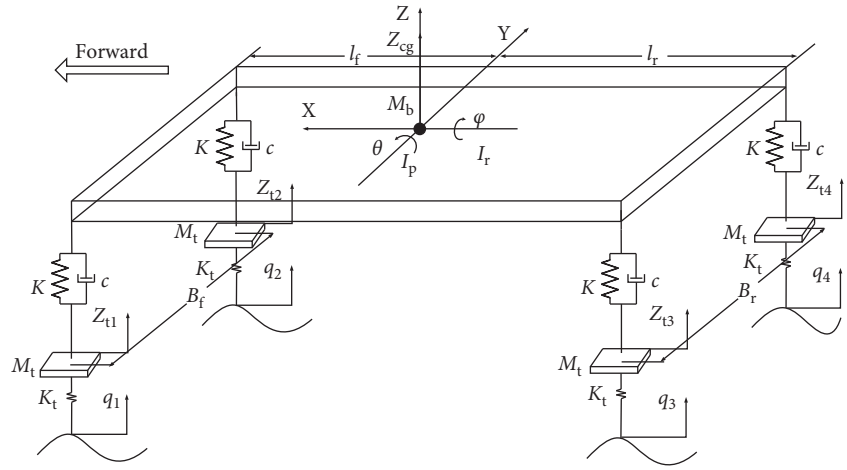

Figure 1: A physical model of vehicle body and wheels for vertical vibration.

In which,

$$\begin{cases} F_i = K \cdot f_{di} + c \cdot \dot{f}_{di} \, (i = 1, 2, 3, 4), \\ f_{d1} = Z_{t1} - \left(Z_{cg} - l_f \theta + \phi \cdot \dfrac{B_f}{2} \right), \\ f_{d2} = Z_{t2} - \left(Z_{cg} - l_f \theta - \phi \cdot \dfrac{B_f}{2} \right), \\ f_{d3} = Z_{t3} - \left(Z_{cg} + l_r \theta + \phi \cdot \dfrac{B_r}{2} \right), \\ f_{d4} = Z_{t4} - \left(Z_{cg} + l_r \theta - \phi \cdot \dfrac{B_r}{2} \right). \end{cases} \tag{13}$$

The 7 DOF model is simulated under MATLAB/Simulink environment. Based on the equations above, a full car simulation model is built, and its parameters are set according to a test bench as Table 2.

According to the road displacement PSD and its' transfer function given in Equations (6) and (7), the differentials can be calculated and described as

$$\dot{q}(t) = 2\pi n_0 \sqrt{G q(n_0) v} \cdot w(t) - \omega_0 q(t), \tag{14}$$

where $q(t)$ is the time domain signal of $G_q(\omega)$; $w(t)$ is time domain signal of white noise. According to this differential equation, time domain road quarter model can be established in the Simulink environment.

When the vehicle is moving, the left and right wheels are inspired by a different road, but which are not independent of each other.

In [23], Dieter Ammon presents a widely used method for calculating the coherence of left and right road $\gamma(n)$ as

$$\gamma(n) = \left[1 + \left(\frac{n T_w^{\alpha_r}}{n_p} \right)^2 \right]^{-p_r}, \tag{15}$$

where α_r is the influence range of wheel track on the density of coherence function; n_p is the slope at the inflection point of the coherence function; and p_r is the position of this point, respectively. T_w is wheel track.

Table 2: Parameters for the full car model.

Parameter	Value
Body mass M_b	2039 kg
Wheel mass M_t	53.64 kg
X-axis rotational inertial I_r	586 kg·m^2
Y-axis rotational inertial I_p	3492 kg·m^2
Tire stiffness K_t	260 kN/m
Front wheel tread B_f	1.515 m
Rear wheel tread B_r	1.515 m
Distance from centroid to rear axle l_r	1.321 m
Distance from centroid to front axle l_f	1.417 m
Damping coefficient in compression travel c_{up}	1800 N·s/m
Damping coefficient in stretch travel c_{dn}	2800 N·s/m
Spring stiffness K	140 kN/m

When the road at the front left wheel is determined, the right side of the road can be calculated by the transfer function whose means values equal to the coherence function above. If ignoring the turning condition, it can be considered that the rear wheels passing through the road are the same with the front wheels. According to hysteresis between the front and rear wheels, the rear side of the road can also be calculated. So, the vertical displacement excitations of four wheels can be written as follows:

$$\begin{cases} \dot{q}_1(t) = 2\pi n_0 \sqrt{G_q(n_0) v} \cdot w(t) - \omega_0 q_1(t), \\ q_2(t) = L^{-1}\left[H(s) L(q_1(t)) + (1 - H(s)) S_\omega \right], \\ q_3(t) = L^{-1}\left[e^{-(ls/v)} L(q_1(t)) \right], \\ q_4(t) = L^{-1}\left[e^{-(ls/v)} L(q_2(t)) \right], \end{cases} \tag{16}$$

where l is wheelbase in m, v is vehicle speed in m/s, and L and L^{-1} mean Laplace transform and inverse Laplace transform.

Figure 2 shows the generated random road profiles at each wheel classified by ISO as "A" using Equation (16). And the smoothed PSD of roads on the front left wheel and front right wheel are illustrated in log-log scale in Figure 3, which also contains the roughness indices information classified by ISO.

According to Equation (11), the mean square value of unsprung mass acceleration is related to the road roughness

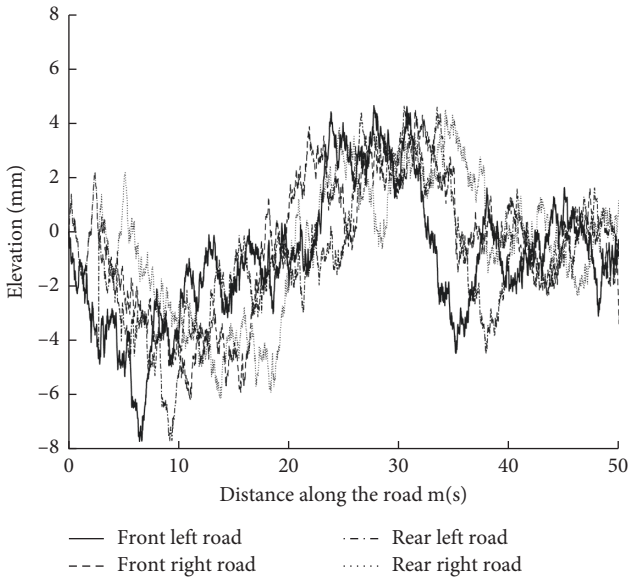

Figure 2: Class "A" road profile at each wheel.

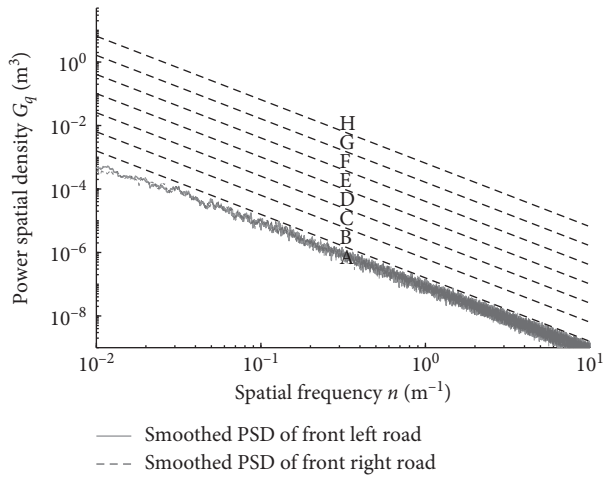

Figure 3: Road roughness classification and smoothed PSD of front left and right road generated.

and the vehicle speed. And if the sampling frequency is infinite and sampling time is infinitely long, the PSD of white noise is supposed to be equal to 1 at the arbitrary frequency. Based on this, when the vehicle parameters are determined, the mean square of unsprung mass acceleration divided by vehicle speed should have obviously positive correlation relationship with road roughness. Therefore, the mean square of unsprung mass acceleration divided by vehicle speed can be used as the parameter to classify the road roughness, which records as ADV (acceleration divided by velocity) here.

But in reality, the sampling frequency and sampling time are limited. Therefore, the PSD of white noise cannot be identically equal to 1, and its value is closely related to the sampling frequency and time. Considering the inherent amplitude-frequency characteristics of the vehicle suspension, the ware number ratios of the road studied in this paper range between 0.01 and 10 m^{-1}. In the case of vehicle speed ranging from 10 to 30 m/s, the time-frequency range is 0.3~300 Hz. This range is sufficient to cover the important frequencies of the vehicle. Therefore, the sampling frequency here should be higher than 600 Hz according to Shannon theorem. In consideration of the simulation environment, the sampling frequency is decided to be the reciprocal of simulation's fundamental sample time as 1000 Hz. This is also a sampling frequency which many single-chip AD conversions can easily reach.

3. Relationship between ADV Values and Time-Window

The ADV values can be calculated by the following equation with a moving window:

$$\mathrm{ADV} = \frac{1}{k}\sum_{i=1}^{k}\frac{1}{ftv}\sum_{n=N-ft}^{N}\ddot{Z}_{ti}(n)^2, \tag{17}$$

where f is sampling frequency that has already been determined as 1000 Hz and t is the time-window length in s. The ADV values are calculated by a window length of $f \times t$ points and a window overlap of $f \times t - 1$ points. k is the number of vehicle wheels. And here, all unsprung mass accelerations are taken into consideration for they can be used as a simple mean filter to offset some effect of small stones or pits of the road in practical application, and in this paper, k is equal to 4. As it can be seen from the equation, this calculation uses the mean values of unsprung mass acceleration of four suspensions and then computes the ADV values using all the data points during time-window t. It can be predicted that when the time-window t becomes shorter, the ADV values will fluctuate more greatly, because the uncertainty of PSD values of white noise under each frequency corresponding to the data covered by time-window is larger.

Figure 4 shows the ADV values which are calculated with different time-windows ranging from 1 to 8 seconds under the same condition with Figure 2.

It clearly shows that the ADV values fluctuate more sharply with narrower time-window. Moreover, the length of time-window has little effect upon the mean values of ADV while significantly increases the response hysteresis of ADV values on road roughness, which presents as a slow climb curve at the beginning of the figure.

For further revealing the influence of time-window on the fluctuation of ADV values, simulations under different time-windows lasting 1000 seconds were carried out. After abandoning the initial date of hysteresis sections, the distributions of ADV values of the 1000 seconds are calculated. The results are shown in Figure 5.

As it can be seen from Figure 5, the length of time-window has no effect on the mean values of ADV. In this case, under A class road condition, no matter what the time-window is, the mean values of ADV always equal 0.5947 for a sufficiently long period of simulation. Figure 6 shows how the mean values and RMS (root mean square) values at different time-windows of ADV change when the road

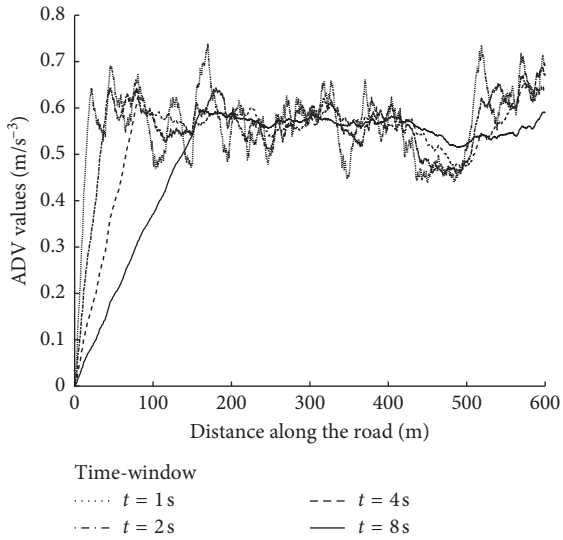

Figure 4: ADV values calculated at different time-window.

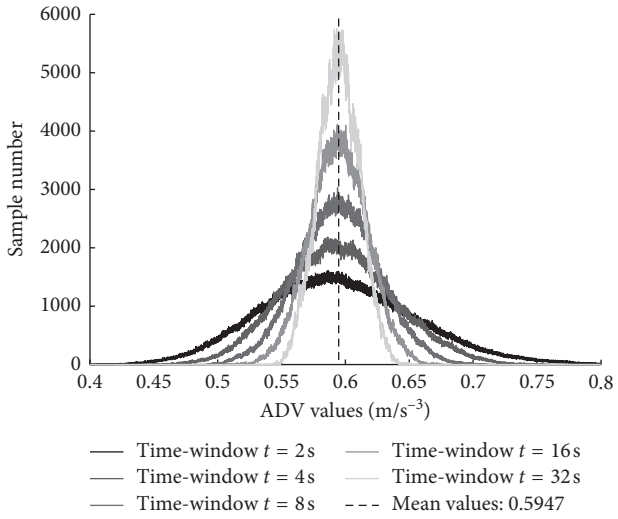

Figure 5: Statistics of ADV values calculated at different time-window.

roughness coefficient $G_q(n_0)$ changes. In Figure 6, which was set as log-log axes, it is easy to find that both the mean values and RMS values of ADV have a high linear relationship with road roughness coefficient $G_q(n_0)$.

Also, time-window has a significant influence on the RMS values of ADV, the RMS values of ADV decreases with the extension of time-window. As the square of RMS values, the mean square values of ADV have the same rule. Given the road elevation obeys normal distribution, the unsprung mass acceleration as the response to road elevation should also obey the normal distribution. Therefore, the mean square values of unsprung mass acceleration should obey χ^2 distribution. But when the sample size is large enough, it can be considered as a normal distribution. Therefore, to reduce the calculation, the mean square values of unsprung mass acceleration are regarded as a normal distribution here.

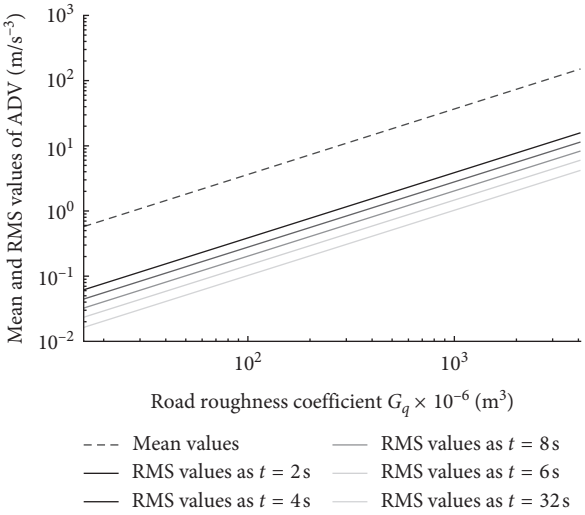

Figure 6: How the mean values and RMS values of ADV change with road roughness at different time-window.

In a normal distribution, about 68% of values drawn from a normal distribution are within one standard deviation σ away from the mean; about 95% of the values lie within two standard deviations, and about 99.7% are within three standard deviations. This fact is known as the 3-sigma rule. Therefore, if the output value of ADV at a certain time is in the section $(\mu - 3\sigma, \mu + 3\sigma)$, there should be a 99.7% certainty that the current road roughness coefficient is the coefficient corresponding to mean value μ, assuming an ADV computing system, in which the mean values of ADV corresponding to two road roughness coefficients that are μ_1 and μ_2 $(\mu_1 < \mu_2)$, and the root mean square values are σ_1 and σ_2. If $\mu_1 + 3\sigma_1 < \mu_2 - 3\sigma_2$, it can be considered "significantly" that this system is able to distinguish between two road roughness coefficients.

For further elaboration, the road roughness coefficients are chosen as 16×10^{-6} and 20×10^{-6} m^3 and the ADV values are calculated with 2 s and 32 s time-windows in simulation. The results are shown in Figure 7 as follows.

If a calculated ADV value is 0.65 at one time, in a system that using 2 seconds' time-window of data to calculate ADV values to classify the road roughness, it will not be able to judge whether the vehicle is driven on the road with roughness coefficient of 16×10^{-6} or 20×10^{-6} m^3. Because the probability of value 0.65 appearing in both cases is significantly large, it is difficult to say exactly what level the road roughness is corresponding to. In another word, in this situation, a system that working on a 2 seconds' time-window cannot distinguish 25% differences between road roughness coefficients. But the system that is working on a 32 seconds' time-window of data to calculate ADV values to estimate the road roughness can easily determine that the current road roughness coefficient is not at 16×10^{-6} m^3 level. In other words, the longer the time-window is, the more accurate the system will classify the road roughness coefficient and the higher the resolution will be.

The above-discussed content explains that it is necessary to choose the time-window when using the ADV values to

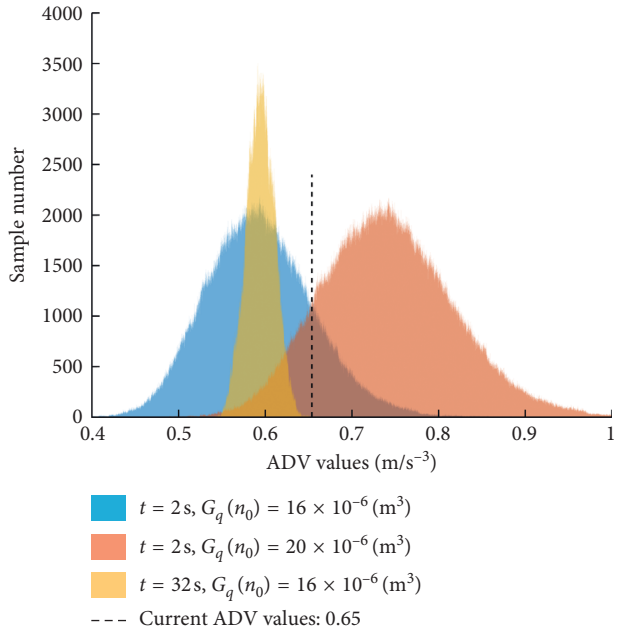

Figure 7: Judgment of systems with different time-window while facing with a certain ADV value.

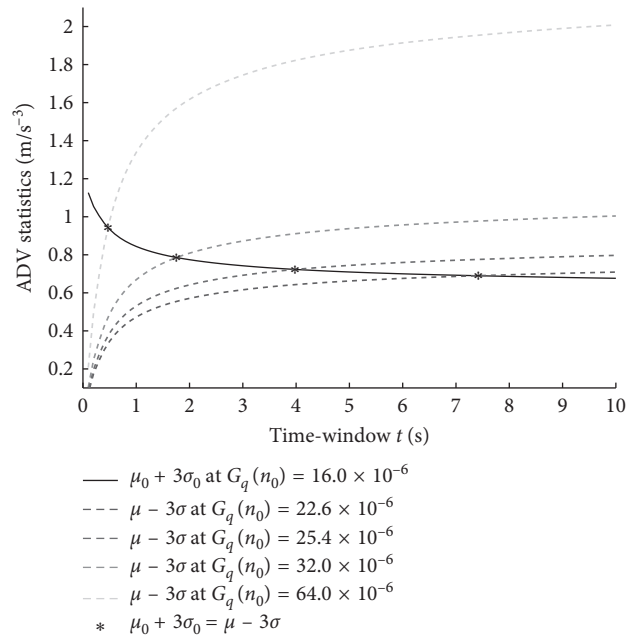

Figure 8: The results of minimum time-window length selection.

classify the road roughness. However, there is a contradiction in time-window: the longer the time-window, the higher the accuracy of estimation, but the delay will be intensified and the shorter the time-window, the faster the reaction is, but less the accuracy will be.

Considering the road roughness coefficients array in exponential form and the road roughness classification has the contradiction to classify accuracy, it is necessary to divide the original road roughness into more accuracy levels in exponential form to satisfy the requirements of vehicle control systems asking for accurate road roughness level information. For "A" and "B" classes of road, they can be divided into two sections whose central roughness coefficient is 16×10^{-6} and 64×10^{-6} m^3 or divided into three sections whose central roughness coefficient is 16×10^{-6}, 32×10^{-6}, and 64×10^{-6} m^3, or divided into four sections, etc. The more sections the road roughness is divided into, the smaller the gap between each section will be and the longer the time-window should be. According to the 3-sigma rule, the time-window lengths that can divide "A" and "B" classes of the road into 2~5 sections and can be distinguished by 99.7% probability are calculated. The results are shown in Figure 8.

In Figure 8, the black solid line is a set of data points that represent the sum of μ_0 and $3\sigma_0$, in which μ_0 and σ_0 are mean and mean square values of ADV calculated under road roughness coefficient $G_q(n_0) = 16 \times 10^{-6}$ m^3 with different time-windows from 0.1 to 10 seconds in step length 0.1 seconds. The lines in points are differences of μ and 3σ, in which μ and σ are mean and mean square values of ADV calculated under different road roughness coefficients with same time-windows above, and those road roughness coefficients are the minimum coefficient numbers that the classification system should distinguish with road roughness coefficient of 16×10^{-6} m^3 if dividing "A" and "B" classes of road into 2~5 sections by geometric progression. The gray "$*$" marks point out where the black solid line has a cross with those point lines. And the corresponding lateral axis numbers of gray "$*$" marks are the minimum time-window lengths that a classification system should use to distinguish each section by 99.7% probability. In operational application, the time-window length can be chosen as long as 0.5 seconds, 1.8 seconds, 4.0 seconds, or 7.5 seconds for accurate classification according to Figure 8 and the final time-window length can be decided on the balance between the control systems' demands of accuracy and tolerances of delay. In this paper, the 7.5 seconds of time-windows length is selected on the purpose of discovering the accuracy performance of this method. Because the first five classes (A~E) of roads are important in practice and the "F," "G" and "H" classes of roads are rarely see, this method is only applied on "A"~"E" classes of roads, and if "A" to "B" classes of roads are divided into 5 sections by geometric progression, the whole "A" to "E" classes of road can be divided into 17 sections by geometric progression and 7.5 seconds of time-windows length is long enough to make a distinction between each of those sections according to Figure 8.

4. Analysis of the Variation of ADV Values with Suspension Parameters

In this paper above, some studies on how to calculate the ADV values and how to choose the sampling frequency and time-window are conducted. But according to Equation (11), it can be found that the mean square values of unsprung mass acceleration of vehicle suspension system are not only related to road roughness, sampling frequency, and time-window in reality, but also has a direct relationship with the amplitude-frequency characteristics of vehicle suspension itself.

With wide use of semiactive suspension, in a vehicle suspension system, only the sprung mass, spring stiffness, and damping coefficient can be changed considerably. Among the three of them, the variation of the spring stiffness is only possible for the semiactive suspensions with air spring capable of height adjustment. However, variable damping coefficient is easier to achieve and common in semiactive suspension, and the variation of damping coefficient is very large. Also, the variation of sprung mass of vehicle itself is significant. Therefore, this paper temporarily overlooks the situation that in a vehicle equipped with air spring in which the stiffness of air spring changes when vehicle height changes, further study is done on the relationship of ADV values with sprung mass and damping coefficient only. The mean values and RMS values of ADV are calculated under A~D classes of road when the sprung mass ranges from 2039 to 4078 kg, which is wide enough to cover the no-load and full-load condition of this test bench. The results show as follow.

Where M_{b0} is initial sprung mass 2039 kg, M_b is current sprung mass in kg, μ_0 and σ_0 are mean and RMS values of ADV under initial sprung mass at A~D classes of road, μ and σ are mean and RMS values of ADV under current sprung mass at A~D classes of road.

Figure 9 shows that both mean values and RMS values have little to do with sprung mass. Even when the sprung mass becomes two times of original sprung mass, the difference between mean and RMS values' changes is less than 1%. Considering the influence of sprung mass on ADV values is very small, no further research was carried out on this topic.

As for damping coefficient, the variation range is much larger. This paper involves dampers with damping coefficients ranging from 1800 to 9300 N·s/m. Based on this, the mean and RMS values of ADV are calculated under A~D classes of road. Figure 10 shows the relationship between damping coefficient and ADV values.

As it can be seen from Figure 10, when the damping coefficient becomes larger, the mean values of ADV are gradually reduced, and the changing amplitude is large. The damping coefficients and the mean values of ADV seem to have a certain inverse proportion relationship.

By calculating the transfer function of the suspension, the influence of damping coefficient on ADV values can be determined, but it requires a large amount of calculation and involves many parameters. Therefore, it is burdensome in actual operation. In consideration of this and to ensure the stability of calculated ADV values in the case of large variation of damping coefficient and the positive relationship with road roughness, the relationship between damping coefficient and ADV values is fitted. And based on the fitted function, the correction function of ADV is determined to ensure the ADV values stay constant when the damping ranges.

Taking the line drew under $G_q(n_0) = 16 \times 10^{-6}\,\mathrm{m}^3$ as a benchmark, using the curve fitting tool in MATLAB, choosing "Rational" method with numerator degree and denominator degree equal to 1. The fitting result is as follows with correlation coefficient equal to 1.

$$\mu = \frac{0.01917c + 1252}{c - 66.74}. \tag{18}$$

Accordingly, the modified ADV values can be calculated as

$$\mathrm{ADV}_{\mathrm{mod}} = \frac{c - 66.74}{0.01917c + 1252}\,\mathrm{ADV}\mu_0, \tag{19}$$

where μ_0 is mean value of ADV calculated under $G_q(n_0) = 16 \times 10^{-6}\,\mathrm{m}^3$ and $c = 1800$ N·s/m condition. According to Equation (19), the modified ADV values can be calculated.

To verify the feasibility of this method, Figure 11 shows the errors of mean values μ and RMS values σ of modified ADV compared with μ_0 and σ_0. Figure 11 shows that the mean values of modified ADV change a little with the damping coefficient. Basically, the variation level is only 0.7%. Meanwhile, the RMS values of modified ADV keep decreasing with the increase of damping coefficient. It is good news that the classification system can reduce the probability of making the first kind of error.

In suspension system researches, it is usually assumed that the pressure and stiffness of tire are not changing. But the tire pressure can change about ±5% between summer and winter, that makes the tire stiffness can change about ±5%, which can obviously affect the accuracy of classification results. Thus, another correction function can be calculated by the same way as damping's, and the actual tire pressures of each tire can be obtained via TPMS (Tire Pressure Monitoring System) in realty. But doing the same thing twice is not necessary, so this work is left to be done for the researchers who want to take the tire stiffness into consideration.

All the preliminary work has been completed on how to use the ADV value to classify road roughness. The sampling frequency and time-window length are determined to 1000 Hz and 7.5 seconds, and the correction function can be used to calculate the appropriate ADV values under the change of damping coefficient.

In addition, according to the resolving power of modified ADV values calculated under above conditions, the road roughness is divided into 17 sections, as shown in Figure 12 in the log-log scale.

In Figure 12, the red parts are the intersection of ADV values and corresponding road roughness. The green lines indicate the center of each road roughness section while the blue lines represent the ADV values section's center.

5. Online Road Roughness Classification System

The road roughness and ADV values have obvious linear mapping relationship as shown in Figure 12. A neural network is adopted as road roughness classification mapping module in this paper to improve the adaptability and expansibility of classification.

Because the road roughness is divided into 17 sections according to the resolving ability of chosen ADV values, the

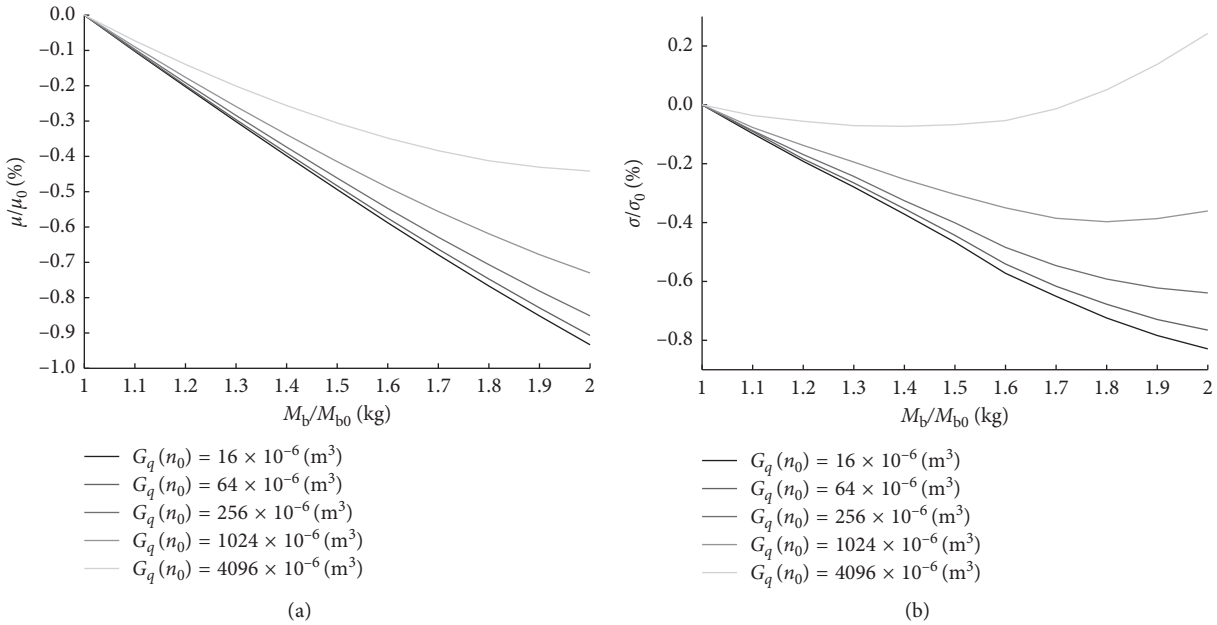

Figure 9: How sprung mass affects ADV values.

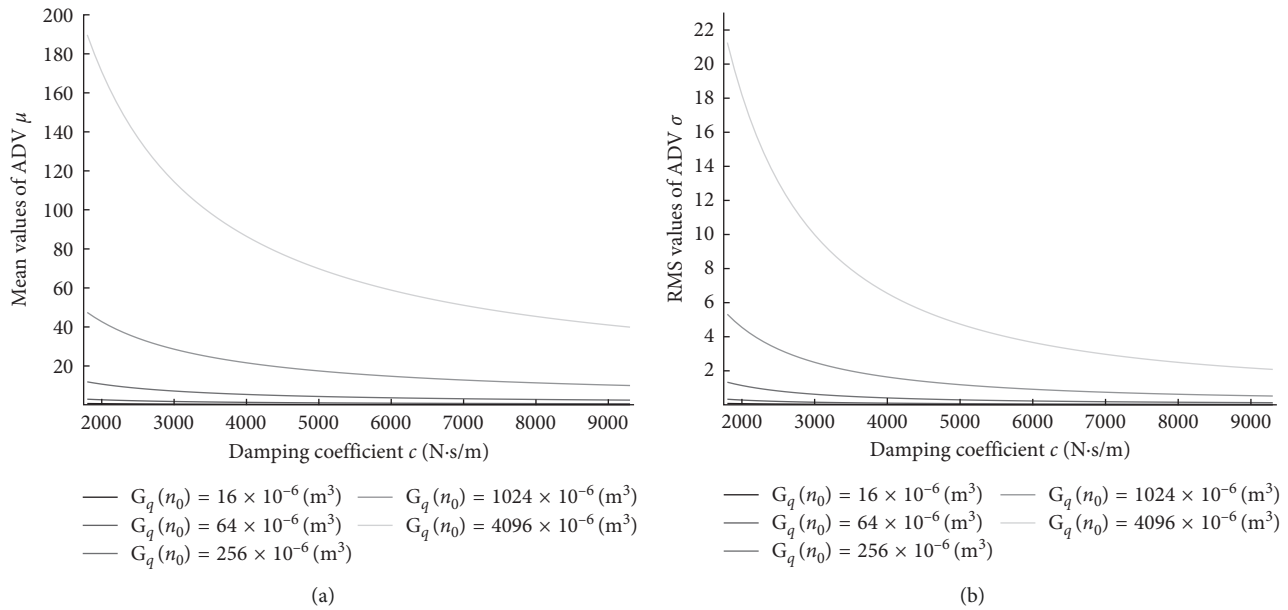

Figure 10: How damping coefficient affects ADV values.

training data can be generated by generating different ADV values and determining which section it belongs to. Support Vector Machine (SVM) or k-Nearest Neighbor (kNN) are good classifiers but need quite amount of calculation, which will reduce the stability and accuracy of this system considerably. Thus, a neural network is chosen to be a suitable classifier to get the linking between ADV values and road roughness. In MATLAB/nprtool environment, a two-layer feed-forward network with sigmoid output neurons can be trained with the training data.

A test was designed to evaluate the performance of the neural network classifier on road roughness among 17 sections. Each road roughness section has a duration of 3600 seconds at constant vehicle speed at 20 m/s with damping coefficient in compression travel and stretch travel 1800 and 2800 N·s/m. The classification error times of this trained network at each road roughness section are shown in Table 3.

From Table 3, it can be seen that the neural network works well on different kinds of roads, and its classification error degrees are mostly less than 0.3%, an error degree limit that is within the designed range. It preliminarily proves that this online road roughness neural network classifier can work smoothly under the fixed working condition and its accuracy is guaranteed.

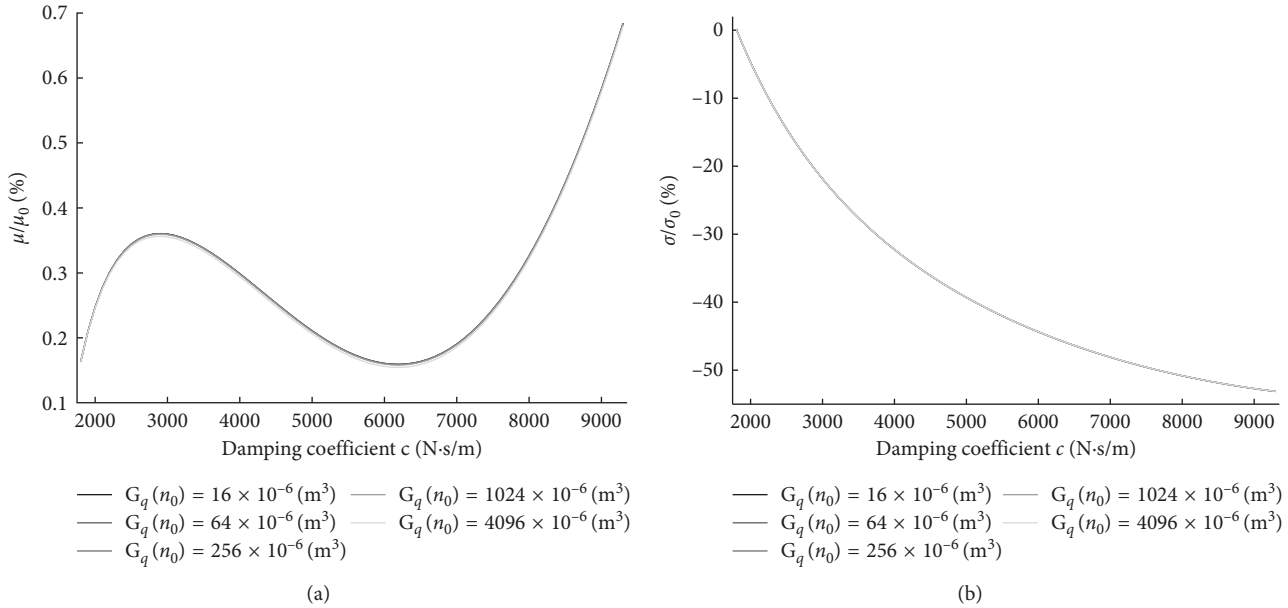

Figure 11: The characteristics of modified ADV values compare with the original.

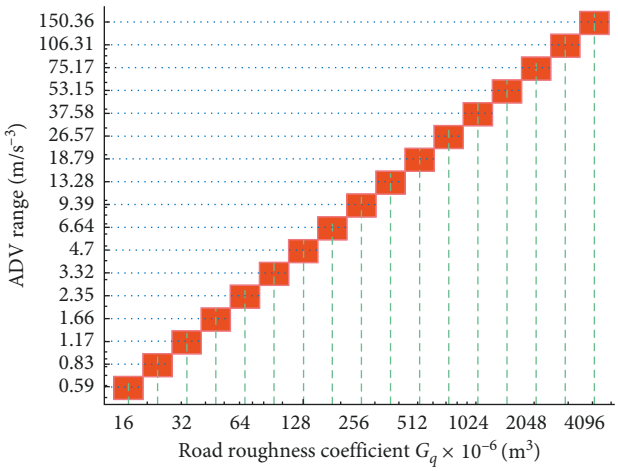

Figure 12: The mapping relationship between road roughness and ADV values.

To evaluate the performance of this classifier under variable conditions, a road with random roughness among 17 sections was established, and each section has a duration of 600 seconds. Also the vehicle speed ranges from 10 to 30 m/s in sine law with a cycle of 2000 s/cycle, while all the dampers are controlled by Sky-Hook controller with first-level damping coefficients in compression travel and stretch travel being 1800 and 2800 N·s/m and second-level damping coefficients in compression travel and stretch travel being 4800 and 9300 N·s/m. Figure 13(a) shows the classification condition including the road elevations at the left front wheel of each section, vehicle speed, and a fragment of damping coefficients of left front damper that are controlled under Sky-Hook. Figure 13(b) shows the ADV values that are calculated under the working conditions shown in Figure 13(a) and the upper and lower limits of ADV values for different sections of road roughness. The road roughness classification results and corresponding road roughness levels are shown in Figure 13(c).

Table 3: Error times of road roughness classification at different roughness sections in percentage.

$G_q(n_0) \times 10^{-6}$ m^3, geometric average	Underestimate %	Overestimate %
16	0.10	0
23	0.00	0.18
32	0.05	0.29
45	0.03	0.22
64	0.11	0.22
91	0.05	0.21
128	0.08	0.18
181	0.08	0.24
256	0.07	0.17
362	0.05	0.17
512	0.00	0.23
724	0.13	0.18
1024	0.03	0.19
1448	0.09	0.17
2048	0.04	0.21
2896	0.00	0.18
4096	0.06	0.15

Figure 13 shows that under changing circumstances, the stability and reliability of neural network that using ADV to classify road roughness level are still acceptable. In the process of variable speed driving, this system can still well classify the road roughness level.

6. Conclusions

This paper has developed a method for stable online road roughness classification so that some of the control systems on the vehicles can acquire necessary road information to

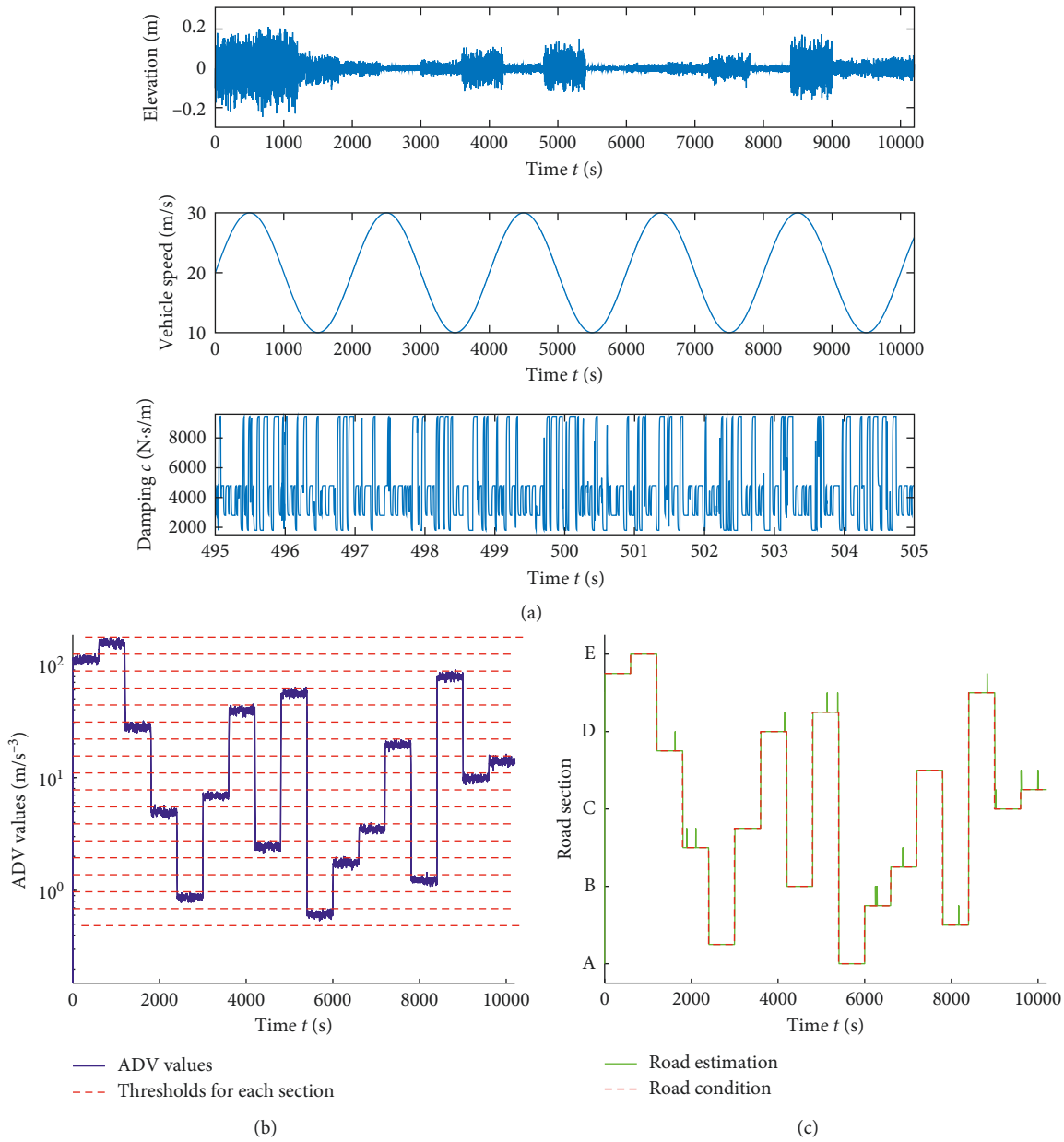

Figure 13: The performance of road classification on variable conditions. (a) Road classification working condition. (b) ADV values. (c) Road roughness classification results and corresponding road roughness levels.

improve the performance of vehicles in different road conditions. The theoretical analysis shows that the mean square values of unsprung mass acceleration divided by vehicle speed have an obvious linear relationship with road roughness coefficient. The use of unsprung mass acceleration offers some advantages as the quality of unsprung mass is constant, and the variation of sprung mass or vehicle body height has little influence on it. Also, using unsprung mass acceleration divided by vehicle speed as information source makes the classification and vehicle speed decouple.

Based on this, the sampling frequency as 1000 Hz of unsprung mass acceleration was selected in consideration of inherent amplitude-frequency characteristics of the vehicle suspension and feasibility, and the equation with a sliding window for calculating ADV values was given. The relationship between the length of time-window, the distribution, and statistical parameters were studied. According to the distribution and 3-sigma rule, a suggestion of the shortest time-windows lengths under different classification accuracies is given, and a 7.5 seconds long time-window was chosen as a performance indicator to show the accuracy performance of this methods. To just distinguish each level of roads in ISO standard in the expense of accuracy requirement of road roughness classification, the time-windows length can be set as short as 0.5 seconds, while the correct distinguishing probability stays at 99.7%.

After determining how to calculate the ADV values, the relationships between the suspension parameters (sprung

mass and damping coefficient) and the statistical parameters (mean and RMS values) of ADV were analyzed. Accordingly, a correction function was determined to ensure the ADV values remain when the damping ranges. After the correction, the modified ADV values showed a good stability toward varying damping coefficient.

Since the modified ADV values are none related to vehicle speed and suspension parameters, a neural network classifier was established. The performance of the neural network classifier has been demonstrated for varying vehicle speed, road roughness levels, and different damping coefficients controlled by Sky-Hook control. The classifier performance remains stable, and the sum of its overestimate errors and underestimate errors is mostly smaller than it was designed to be.

Data Availability

The data used to support the findings of this study are included within the article.

Conflicts of Interest

The authors declare that they have no conflicts of interest.

Acknowledgments

The authors acknowledge the support from the National Natural Science Foundation of China (Nos. 51575241 and 51305111); the Six Talents Peak Foundation of Jiangsu Province (No. 2012-ZBZZ-030); the Natural Science Foundation of Jiangsu Province (No. BK20131255); Key Research and Development Plan of Hunan Province (No. 2017GK2204); and Hengyang Science and Technology Development (No. 2017KJ158).

References

[1] S. Yongjun, L. Xiandong, and Y. Shaopu, "Research on the application of optimal control theory on parameters optimization of vehicle suspension," *Journal of Low Frequency Noise, Vibration and Active Control*, vol. 22, no. 4, pp. 253–263, 2003.

[2] J. C. Tudón-Martínez, S. Fergani, S. Varrier et al., "Road adaptive semi-active suspension in an automotive vehicle using an LPV controller," *IFAC Proceedings Volumes*, vol. 46, no. 21, pp. 231–236, 2013.

[3] R. Burdzik, "Identification of structure and directional distribution of vibration transferred to car-body from road roughness," *International Congress on Telecommunication and Applications Icta*, vol. 16, no. 1, pp. 324–333, 2014.

[4] B. Goenaga Silvera, L. G. Fuentes, and O. Mora, *Effect of Road Roughness and Vehicle Speed on Dynamic Load Prediction and Pavement Performance Reduction*, The National Academies of Sciences, Engineering, and Medicine, Washington, DC, USA, 2017.

[5] P. Liu, B. Liu, T. Dong et al., "Road roughness identification and shift control study for a heavy-duty powertrain," *Energy Procedia*, vol. 105, pp. 2885–2890, 2017.

[6] Y. C. Qin, L. Reza, and L. Gu, "The use of vehicle dynamic response to estimate road profile input in time domain," in *Proceedings of ASME Dynamic System Control Conference (DSCC)*, San Antonio, TX, USA, October 2014.

[7] N. Abulizi, A. Kawamura, K. Tomiyama, and S. Fujita, "Measuring and evaluating of road roughness conditions with a compact road profiler and ArcGIS," *Journal of Traffic and Transportation Engineering*, vol. 3, no. 5, pp. 398–411, 2016.

[8] N. Lushnikov and P. Lushnikov, "Methods of assessment of accuracy of road surface roughness measurement with profilometer," *Transportation Research Procedia*, vol. 20, pp. 425–429, 2017.

[9] Y. Balaram and M. Mostert, "Lessons learnt from the measurement of gravel road roughness in Kwazulu-Natal," in *Proceedings of 5th SARF/IRF Regional Conference, 2014*, Pretoria, South Africa, September 2014.

[10] P. Kumar, P. Lewis, C. P. McElhinney, and A. A. Rahman, "An algorithm for automated estimation of road roughness from mobile laser scanning data," *The Photogrammetric Record*, vol. 30, no. 149, pp. 30–45, 2015.

[11] Z. Zhang, F. Deng, Y. Huang, and R. Bridgelall, "Road roughness evaluation using in-pavement strain sensors," *Smart Materials and Structures*, vol. 24, no. 11, article 115029, 2015.

[12] K. Laubis, V. Simko, A. Schuller et al., "Road condition estimation based on heterogeneous extended floating car data," in *Proceedings of the 50th Hawaii International Conference on System Sciences*, Waikoloa Village, HI, USA, January 2017.

[13] V. Douangphachanh and H. Oneyama, "Estimation of road roughness condition from smartphones under realistic settings," in *Proceedings of 2013 13th International Conference on ITS Telecommunications (ITST)*, pp. 433–439, IEEE, Tampere, Finland, November 2013.

[14] J. C. Tudon-Martinez, S. Fergani, O. Sename et al., "Online road profile estimation in automotive vehicles," in *Proceedings of 2014 European Control Conference (ECC)*, pp. 2370–2375, IEEE, Strasbourg, France, June 2014.

[15] Y. Li, B. Yong, H. Wu, R. An, and H. Xu, "Road detection from airborne LiDAR point clouds adaptive for variability of intensity data," *International Journal for Light and Electron Optics*, vol. 126, no. 23, pp. 4292–4298, 2015.

[16] H. M. Ngwangwa and P. S. Heyns, "Application of an ANN-based methodology for road surface condition identification on mining vehicles and roads," *Journal of Terramechanics*, vol. 53, pp. 59–74, 2014.

[17] H. M. Ngwangwa, P. S. Heyns, H. G. A. Breytenbach, and P. S. Els, "Reconstruction of road defects and road roughness classification using Artificial Neural Networks simulation and vehicle dynamic responses: application to experimental data," *Journal of Terramechanics*, vol. 53, pp. 1–18, 2014.

[18] Y. Du, C. Liu, D. Wu, and D. Jiang, "Measurement of international roughness index by using-axis accelerometers and GPS," *Mathematical Problems in Engineering*, vol. 2014, Article ID 928980, 10 pages, 2014.

[19] J. C. Tudon-Martinez, S. Fergani, O. Sename, J. J. Martinez, R. Morales-Menendez, and L. Dugard, "Adaptive road profile estimation in semiactive car suspensions," *IEEE Transactions on Control Systems Technology*, vol. 23, no. 6, pp. 2293–2305, 2015.

[20] M. Doumiati, J. Martinez, O. Sename, L. Dugard, and D. Lechner, "Road profile estimation using an adaptive Youla–Kučera parametric observer. Comparison to real profilers," *Control Engineering Practice*, vol. 61, pp. 270–278, 2017.

[21] P. Gaspar, Z. Szabo, and J. Bokor, "Identification of vehicle models and road roughness estimation," *IFAC Proceedings Volumes*, vol. 37, no. 8, pp. 257–262, 2004.

[22] Y. Zhisheng, *Automotive Theory*, China Machine Press, Beijing, China, 5th edition, 2000.

[23] D. Ammon, "Problems in road surface modelling," *Vehicle System Dynamics*, vol. 20, no. S1, pp. 28–41, 1992.